American Journal of Physical Chemistry
2024; 13(1): 1-8
http://www.sciencepublishinggroup.com/j/ajpc
doi: 10.11648/j.ajpc.20241301.11
ISSN: 2327-2430 (Print); ISSN: 2327-2449 (Online)

Effect of the Deposition Potential on Morphology, Nucleation, and Crystal Orientation of Nickel Electrodeposited

Koutouan Desire Martial Abro[1, *], Ali Sanou[1], Edith Kouassi Kwa-Koffi[2]

[1]Industrial Processes, Synthesis, Environment and New Energies Laboratory (LAPISEEN), Felix Houphouët-Boigny National Polytechnic Institute (INP-HB), Yamoussoukro, Côte d'Ivoire

[2]Physical Chemistry Laboratory (LCP), Félix Houphouët-Boigny University, (UFHB), Abidjan, Côte d'Ivoire

Email address:

desire.abro@inphb.ci (Koutouan Desire Martial Abro), ali.sanou@inphb.ci (Ali Sanou),
edithkouassi77@yahoo.fr (Edith Kouassi Kwa-Koffi)

[*]Corresponding author

To cite this article:

Koutouan Desire Martial Abro, Ali Sanou, Edith Kouassi Kwa-Koffi. (2024). Effect of the Deposition Potential on Morphology, Nucleation, and Crystal Orientation of Nickel Electrodeposited. *American Journal of Physical Chemistry*, *13*(1), 1-8.
https://doi.org/10.11648/j.ajpc.20241301.11

Received: December 15, 2023; **Accepted**: December 27, 2023; **Published**: January 8, 2024

Abstract: The works reported in this paper deal with the effects of the electrodeposition potential on the morphology, the nucleation, and the crystallographic features of the nickel electrodeposited from a Watts-type bath. For this purpose, coatings electrodeposited at five different deposition potentials from –0.60 V/Ag/AgCl to –0.80 V/Ag/AgCl were investigated. The morphology of the coatings was studied using scanning electron microscopy, and the current transients were compared to the 2D and 3D theoretical models of nucleation and growth. Then, the diffractograms were plotted as a function of the deposition potential. The results showed that the coatings are uniform when deposited at –0.60 V/Ag/AgCl. The nucleation and growth of coatings all follow the instantaneous models in the potential window of study but switch from 2D to 3D at –0.65 V/Ag/AgCl. These different features of the coatings have been attributed to the hydrogen evolution reaction which represents up to 10 % of the total current at –0.80 V/Ag/AgCl. Besides, the calculation of the texture coefficient extracted from the X-ray diffraction data has indicated the plane (220) as the preferred crystal orientation. Also, the observation of the shifts of the peaks has demonstrated the presence of uniform stress in the electrocoatings deposited from –0.60 V/Ag/AgCl to –0.75V/Ag/AgCl. Above, tensile stress appears.

Keywords: Nickel Electrodeposition, Nucleation Model, XRD

1. Introduction

Nickel electroplating is a directed reduction of its metal ions dissolved via an electrolyte onto a cathodically polarized substrate [1]. Nickel electrodeposition consists of the reduction of nickel ions onto a solid substrate submitted to an overpotential via an electrolyte. This cheap, easy-to-handle technique is generally used to improve corrosion [2], oxidation, mechanical, and optical properties of devices through their surfaces coated. Although nickel electrodeposition was practiced decades ago, this technique continues to be used and investigated either for its improvement or its comprehension. Nickel electrodeposition occurs at relatively high overpotential potential i.e. superior to -0.5 V/Ag/AgCl [3] whatever the bath types employed. In fact, among the different baths, the sulfamate bath and the WATTS have gained more attention. Nickel deposits made from sulfonate baths have low mechanical stresses [4], columnar structure [5] and do not recrystallize even after annealing at 300°C for one hour [6]. Moharana *et al.* [7] showed by atomic force microscopy that sulfamate baths produce rougher nickel coatings than those obtained from the WATTS bath [8]. Concerning the WATTS bath, which is a combination of nickel sulfate, and nickel chloride in a medium buffered with boric acid, the presence of Cl^- ions increases the activity of nickel ions by participating in the nickel

ion reduction mechanism [9]. More recently, deep eutectic solvents (DES) [10, 11] have also been used to avoid the hydrogen evolution reaction (HER) which challenges the reduction of nickel in aqueous electrolytes. All the electrodeposition conditions employed in deposition impact the performances of the nickel coatings. For example, Bonfrisco *et al.* [12] showed that the oxidation rate of nickel grains grown according to (111) is the slowest. Then, many works have reported the crystal orientation of nickel grains. Almost all of them conclude that the preferential orientation of nickel electrodeposited is (111) [2, 12, 13]. However, the results of Nzoghe-Mendome indicates that the crystal preferred orientation could be due to the substrate [14]. Then, onto cupper, the nickel coating is textured as (220). Likewise, concerning the nucleation and growth, nickel coatings performed by electrodeposition follows generally the instantaneous model proposed by Sharifker and Hill [15, 16] Yet, on vitreous carbon [18], and quartz crystal [17], the mechanism of nucleation and growth is observed to follow progressive model. Thus, the properties of nickel electrodeposited coating are not unequivocal but strongly depend on the process parameters. Thus, the effect of only one parameter on several properties of nickel electrodeposited coating may be more comprehensive. In the present work, the combined effect of the deposition potential on the nucleation and growth as well as the crystal orientation is reported.

2. Materials and Methods

2.1. Materials and Chemicals

All chemicals were used without further purification. Deionized water produced by a Milli Q plus 185 model from Millipore (Zug, Switzerland) has been employed to prepare all the solutions. Coatings were deposited with a three-electrode system where a carbon steel substrate assuming 8.32 ± 0.7 cm^2; and the Ag/AgCl electrode was the working and the reference electrodes respectively. A double sacrificial nickel (Alfa Aesar) anode was used to compensate for the nickel ions in the plating bath. The nickel anodes were disposed of one at each side of the plate steel to ensure a homogeneous electric field and thus metal deposition. The pH was adjusted at 3.7 ± 0.1 by adding H_2SO_4 or NaOH 10 mM. The temperature of the electrolyte was fixed at 50°C by using a thermostatic bath (Pharmacia Biotech). The composition of the Watts-type bath of 50 mL, employed to prepare coatings is summarized in Table 1.

Table 1. *Nickel Watts bath composition and varied-parameters.*

Composition	Values
$NiSO_4$, $6H_2O$ (g/L)	250
$NiCl_2$, $6H_2O$ (g/L)	90
H_3BO_3 (g/L)	30
SDS (g/L)	0.14
$NiSO_4$, $6H_2O$ (g/L)	250

Prior to each experiment, the steel cathodes are cleaned with a 0.5 M oxalic acid $(CHO_2)_2$ solution at 50 °C during 5 min. Then, the pieces are polished successively with abrasive sandpapers and alumina paste (1 micron). Finally, the electrodes were washed with ethanol and deionized water under sonication for 1 min and dried by a nitrogen stream before each electroplating.

2.2. Cyclic Voltammetry and Chronoamperometry

In this work, the AUTOLAB potentiostat/galvanostat (AUT 71755 ECOCHEMIE) coupled to an acquisition computer controlled by the NOVA and GPES software packages was used to record Cyclic voltammetry (CV) and Chronoamerometry (CA). For all experiments, the electrodes were immersed in a 50 mL electrochemical cell and disposed of in a way that the two counter electrodes are in a face-to-face position with respect to the working electrode. The CVs were recorded from the open circuit potential (OCP= – 0.5 V) to – 1.1 V/Ag/AgCl and to 0.1 V/Ag/AgCl at a scan rate of 100 mV/s. Nickel electrocoatings was performed using chronoamperometry for 1 hour. For chosen potentials from – 0.60 V/Ag/AgCl to –0.8V/Ag/AgCl, potentiostatic current transients were plotted through the WATTS bath under an agitation of 500 rpm. Theses curves are also used for the nucleation models determination.

2.3. Coatings Characterization

The nickel coatings morphologies and microstructures were examined by scanning electron microscopy (SEM, Philips XL-30 FEG). The crystal orientations of nickel coatings were solved by X-rays diffraction in 2θ scan from 40 to 100°. The equipment DISCOVER D8, controlled by DIFFRAC and XRD COMMANDER software was used for this purpose. It generates a monochromatic beam of Cu Kα radiation (λ=0.154056 nm) at a voltage of 40 kV and an intensity of 40 mA. The crystal sizes in nm, D_{crist} have been obtained by using the SCHERRER equation [21], Equation (1).

$$D_{crist} = \frac{0.9\lambda}{f_{WHM}.Cos\theta} \quad (1)$$

With λ the wavelength in nm and f_{WHM} the full width at half-maximum of the peak (111) and θ being the diffraction angle.

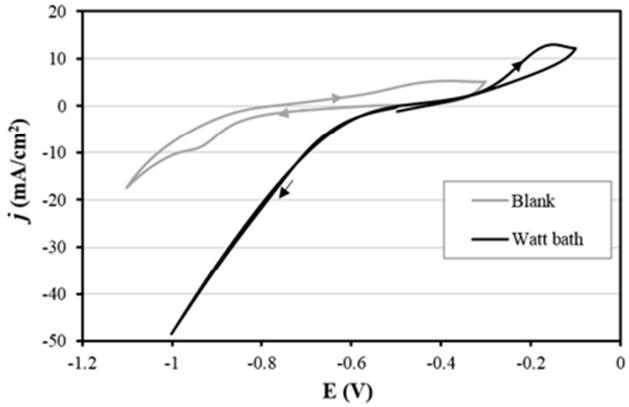

Figure 1. *Cyclic voltammogram in the Blank and in Watt bath at XC100 electrode recorded at 100 mV/s; pH=3.7 and T=50°C.*

3. Results and Discussion

3.1. Cyclic Voltammetry

The voltammetric response in the blank electrolyte and in the nickel Watts bath is shown in Figure 1.

In the blank a reduction plateau relative to proton reduction appears for − 0.93 V followed by the reduction of water molecule into dihydrogen. The peak beginning around – 0.6 V is guessed to be due to a differential airing oxidation since this potential does not correspond to any electroactive species. In the Watt bath, nickel reduction begins at a high overpotential namely – 0.63 V as reported in the literature [22, 23]. Nickel reduction does not depict any diffusion plateau because of the high electrolyte concentration and to bath agitation. A crossover, characteristic of metallic ions electrodepositions appears at − 0.72 V [24, 25]. It indicates a nucleation and growth process. Besides, the electrocoating dissolution takes place around − 0.15 V at the reverse scan.

The cathodic current relative to hydrogen evolution indicated by the blank increases with the potential as depicted by Figure 1. The percentage of current density *j* relative to proton reduction in the cathodic process determined during the forward scan can be assess by the ratio R, Equation 2.

$$R = \frac{j_{H^+/H_2}}{j_{Ni^{2+}/Ni}} \times 100 \quad (2)$$

Table 2 presents the evolution of R as a function of the potential.

Table 2. *Ratio R of hydrogen reduction current.*

E(V)	R (%)
− 0.60 V	5.55
− 0.70 V	7.90
− 0.80 V	9.48
− 0.90 V	19.49

The proportion of current density relative to hydrogen evolution increases up to 20% for −0.90 V. At such potential, coatings become powdery [3, 26] and are without technological interest. To avoid the impact of hydrogen reduction on nickel electrodeposition, the potential window of study has been limited to − 0.80 V. At this potential, the hydrogen evolution current ratio is equivalent to less than 10% namely 9.48%.

3.2. Compactness as a Function of Potential

Figure 2 shows the morphology of coatings electroplated at different potentials.

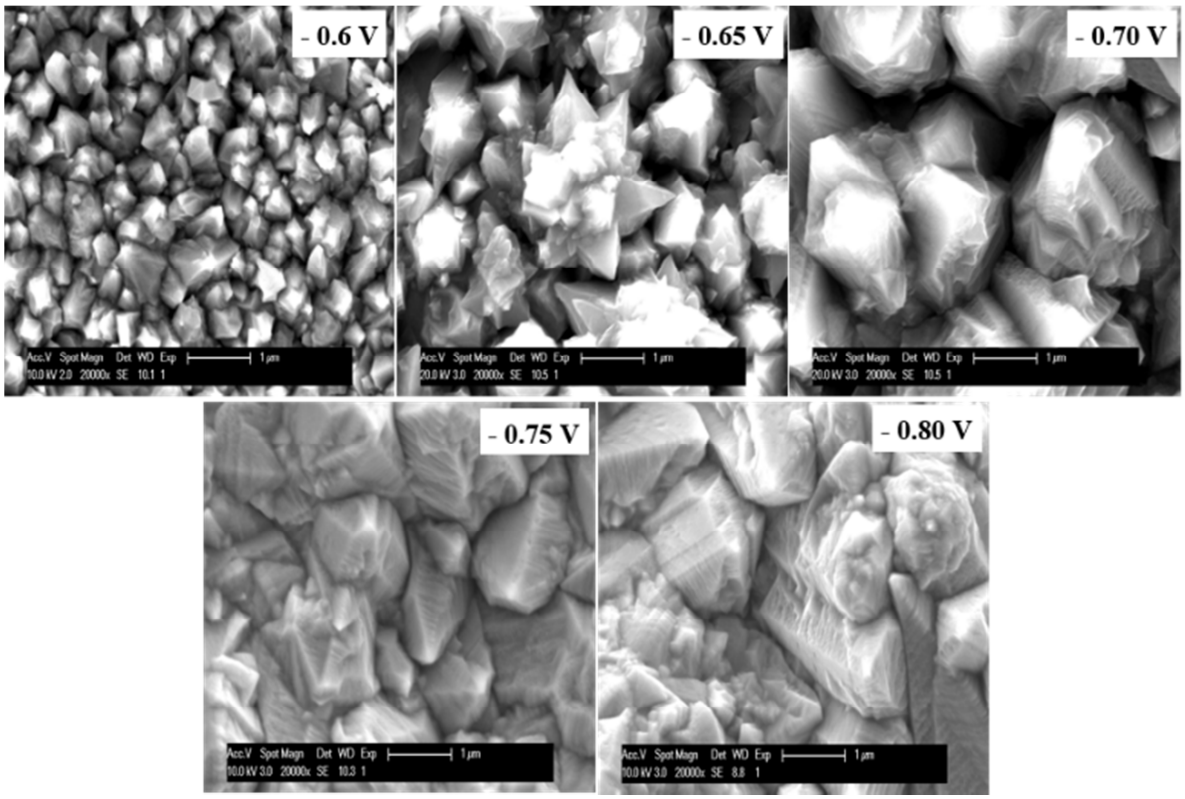

Figure 2. *SEM micrograph of nickel electrodeposited coatings at different potentials. Working conditions: pH = 3.7, agitation rate = 500 rpm and T=50°C.*

As the potential increases, the grain sizes increase. For potentials lower or equal to − 0.70 V, coatings present a uniform, smooth but dispersed structure. But, for higher potentials, the microstructures exhibit compact coatings with pyramidal grains [27].

3.3. Nucleation Study as a Function of Potential

The chronoamperometric current transients presented in Figure 3.

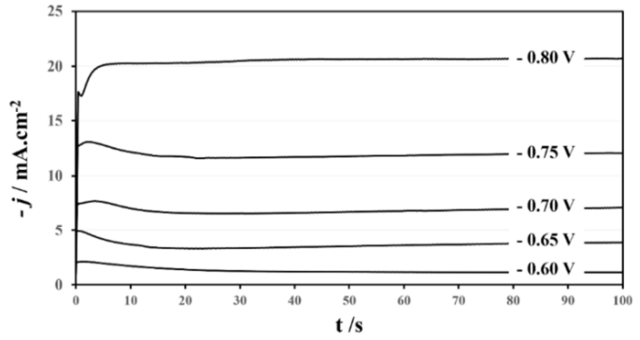

Figure 3. *Potentiostatic transient of nickel electrodeposition operated at different potentials with respect of Ag/AgCl reference. Working conditions: pH = 3.7; agitation rate = 500 rpm and T=50°C.*

Each transient presents a maximum current before decreasing to the limiting current density indicating the that the current density is controlled by the diffusion of nickel ions as stated by the COTTREL equation [28]. This limiting current density increases with the deposition potential E_d suggesting an increase in nucleation rate. Nucleation design the process of formation of the first cluster of metal from liquid phase [20]. For nickel electrodeposition, the nucleation mechanisms can be determined by comparing the experimental chronoamperometric profiles with the theoretical 2D model proposed by Bewick, Fleishmann and Thirsk (BFT theory) [29] and to the 3D model of Scharifker and Hills [15]. The growth model of the deposits is deduced by fitting the non-dimensional curves (i/i_{max}) vs. (t/t_{max}) and $(i/i_{max})^2$ vs. (t/t_{max}) to the theoretical 2D; Equations 3 and 4 and to the theoretical 3D; Equation 5 and 6 nucleation models.

Then, for 2D nucleation process, vs. is fitted to:

$$(i/i_{max}) = (t/t_{max})exp\left[-\frac{1}{2}((t/t_{max})^2 - 1)\right] \quad (3)$$

for instantaneous nucleation, and to

$$(i/i_{max}) = (t/t_{max})^2 exp\left[-\frac{2}{3}((t/t_{max})^2 - 1)\right] \quad (4)$$

for progressive nucleation.

In case of 3D model, vs. is compared to:

$$(i/i_{max})^2 = \frac{1.9542}{(t/t_{max})}\{1 - exp[-1.2564(t/t_{max})]\}^2 \quad (5)$$

for instantaneous nucleation and to

$$(i/i_{max})^2 = \frac{1.2254}{(t/t_{max})}\{1 - exp[-2.3367(t/t_{max})^2]\}^2 \quad (6)$$

for progressive nucleation.

For each fashion, in the instantaneous nucleation, a limited sites on the working surface are rapidly activated for the metal growth from early stage of the deposition while in the progressive nucleation much more growing centres are activated but slowly.

The non-dimensional curves which are compared to the models described aforesaid are plotted in Figure 4.

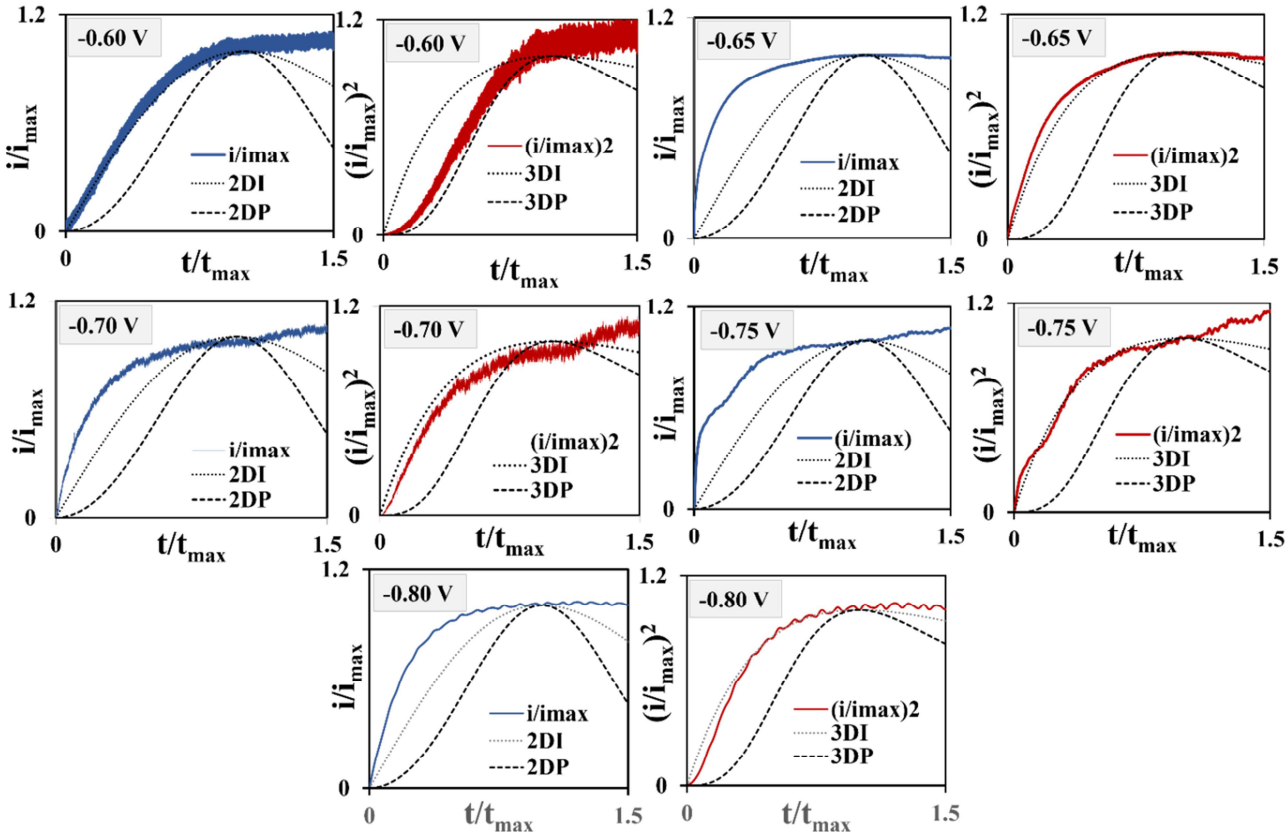

Figure 4. *Comparison of current transients of nickel electrodeposited coatings at different potentials. Working conditions: pH = 3.7; agitation rate = 500 rpm and T=50°C.*

One can clearly distinguish that the crystal growth of coatings deducted from non-dimensional current transients meets a 2DI fashion only for the lowest potential *i.e.* –0.60 V versus Ag/AgCl. At higher potentials, the 3DI growth is followed as reported by Azizi *et al*. [24]. For all curves, the deviation of experimental data from the theoretical ones observed from t/t_{max} 1 is due to the agitation of the plating baths but also to the high concentration in nickel ions of the baths. In fact, the hydrodynamic of the system continuously provides nickel ions in the vicinity of the cathode for electro crystallization. The process is not completely diffusion limited after the early stages of nucleation.

3.4. Crystal Orientation

The crystal plane orientation of the coatings was investigated by X-ray diffraction in the 2θ mode. The results are shown in Figure 5 below.

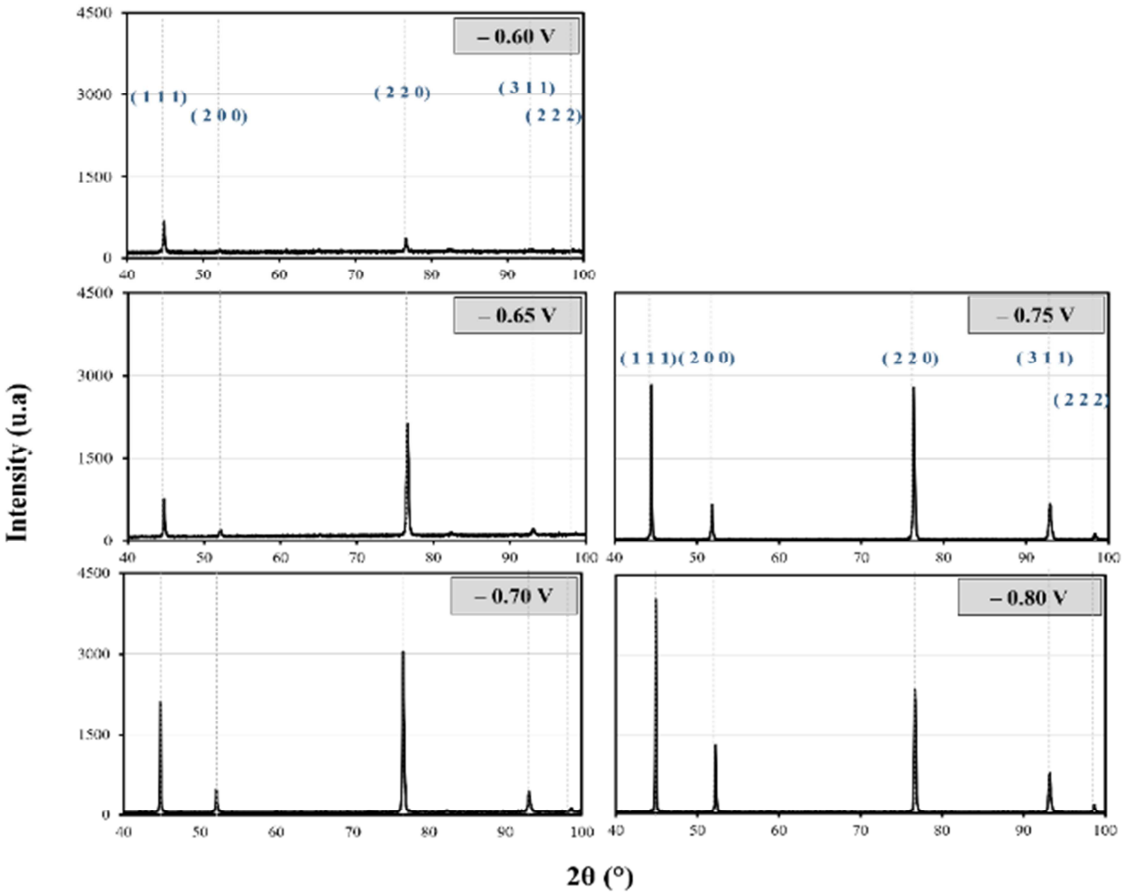

Figure 5. *Diffractograms showing crystal orientation on XC 100 as a function of deposition potential* E_d.

The coatings, deposited by chronoamperometry at different deposition potentials got the same face-centered cubic (FCC) structure. The characteristic peaks and 2θ values extracted from experimental data listed in Table 3 match perfectly with the nickel ICDD 04-0850 card.

Table 3. *Peaks obtained lists with corresponding 2θ.*

No	2θ	Peaks
1	44.5066	(111)
2	51.8459	(200)
3	76.3701	(220)
4	92.9441	(311)
5	98.4456	(222)

The coatings obtained are therefore all polycrystalline with good crystallinity due to the good definition of the peaks; except for the one developed at – 0.60 V regarding the baseline. However, preferential orientations emerge concerning the potentials as reported [30]. As the deposition potential increases, the plane (111) becomes more and more intense unlike peaks representing the plane (2 2 0). The latter increases with the lower overpotentials (-0.60 V; -0.65 V; -0.70 V) and then decreases for the highest (-0.75 V; -0.80 V). As for the planes (200) and (311), their intensities increase but remain low compared to those of the planes (111) and (220). AMBLARD *et al.* [31] have shown that these planes are only the dispersion of (211). Thus, the (111) and (220) planes remain the preferred growth planes for the electrolytic coatings developed in this work, as for metals with the FCC structure [14, 32, 33]. The effect of the potential on the orientation of the nickel electrodeposited films is investigated using the texture coefficient TC (hkl) given by Equation 7 [34].

$$TC\ (hkl) = \frac{I(hkl)/I_0(hkl)}{\frac{1}{N}\sum N\frac{I(hkl)}{I_0(hkl)}} \quad (7)$$

In this equation, I(hkl) represents the experimentally measured intensity, I_0(hkl) is related to the intensities of peaks read on the reference card JCPDS 004-0850 and *N* is the number of diffraction peaks which are 4 *i.e.* (111), (200), (220) and (311). The evolution of TC (hkl) is plotted in Figure 6.

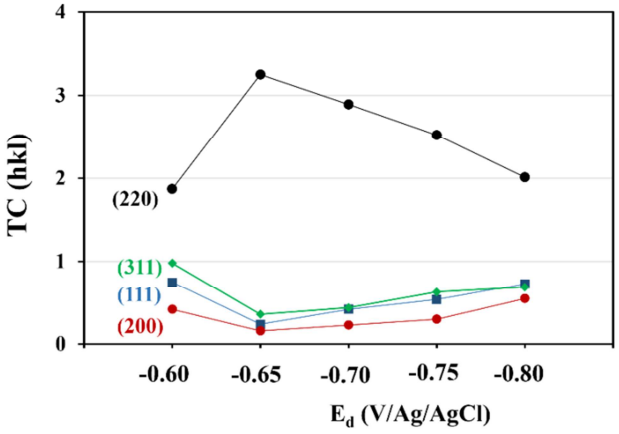

Figure 6. *Evolution of the texture coefficients of coatings as a function of the deposition potential E_d along (111), (200), (220), and (311) planes.*

The evolution of TC (hkl) allows to confirm that the electrodeposited nickel presents a good crystallinity with a preferential orientation plane (220) especially at – 0.65 V/Ag/AgCl where a maximum value is reached. This observation seems to be obvious since the nucleation and growth of the coating mostly follow the 2D model at lower potentials.

According to Cherrnov [35], surfaces consist of terraces, steps, and kinks. In the 3DI nucleation and growth fashion, the surface consists of numerous nuclei islands which may generate a lot of kinks. These kinks increase the probability for new nuclei to establish more bonds which stabilize them onto the growing crystal. Thus, although, the surface energy of (111) is the lowest for FCC nickel crystal as demonstrated by Vitos et *al.* [36], (220) remains preferential. This observation is mainly the result of the surface effect as showed by Nzoghe-Mendome et *al.* [37]. However, the intensity of the plane (220) decreases for more negative deposition potentials. As indicated previously in Table 3, the reduction rate related to proton activity increases with the potential. This proton reduction mechanism involves the adsorption of the intermediate H_{ads} [7]. Thus, the presence of H_{ads} on the cathode surface may block the nucleation and growth sites of stacking of (220) plane and favor growth along over directions. Beyond this, the growth of (111) is favored due to the alkalinization of the cathode/electrolyte interface [38, 39]. In fact, for the same deposition time and the same proton concentrations, for high deposition potentials, more hydrogen ions are involved in reduction reactions so that the proton consumption is higher.

The lattice parameter *a* and the size of the crystallites obtained as a function of the deposition potential were calculated and recorded in Table 4.

Table 4. *Cristal parameters.*

E_d (V/Ag/AgCl)	*a* (A^0)	Crystallites size (A^0)
– 0.60	3.502	399.639
– 0.65	3.515	301.444
– 0.70	3.516	368.518
– 0.75	3.525	397.152
– 0.80	3.512	497.409

The lattice parameter *a* seems to evolve in the same order with the potential until –0.75 V. This suggests the expansion of the crystal lattice with may generate mechanical stresses. This fact is corroborated by the shift in the growth peaks of the planes (220) and (111) showed in Figure 7.

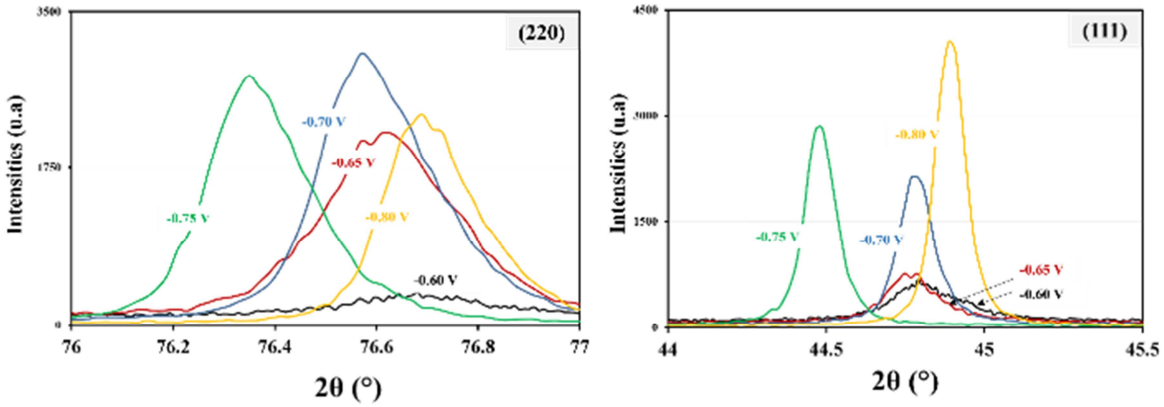

Figure 7. *Shifting the peaks (220) and (111) and as a function of the eposition potential* $\boldsymbol{E_d}$.

From –0.60 V to –0.75 V, the peaks move towards the low values of 2θ. This reflects the existence of uniform stresses in the coating. From –0.75 V, tensile stresses appear with respect to the displacement of the peaks towards the large values of 2θ [40, 41]. At –0.80 V, the hydrogen evolution reaction (HER) lead to smaller crystals. In fact, as the potential increases, the coating may become powdery [14].

Concerning the size of the crystallites, it decreases from – 0.60 V to –0.65 V and then increases as $\mathbf{E_d}$ increases [19]. At – 0.60 V, the reduction of nickel is only just beginning as shown

in the cyclic voltammogram of Figure 1. The corresponding current related to the hydrogen evolution reaction (HER) is low enough to allow the nickel nuclei to grow into a 2D model that goes on unhindered. This results in a smooth and uniform coating (Figure 2). However, when, the potential increases, for –0.65 V, the kinetic of HER increases such that nuclei growth is impeded, and the crystallite sizes decrease before increasing again as a function of the applied potential.

4. Conclusions

In this study, the nucleation and growth models in relationship with the crystallography of the nickel coating as a function of the electrodeposition potential were investigated. SEM images depicted smooth and uniform coatings when –0.60 V/Ag/AgCl is applied. Above, this potential, pyramidal grains are obtained. The comparison of the current transients with the theoretical model has shown that nucleation of nickel is instantaneous in every case but switches from 2D to 3D for deposition potential higher than -0.6 V/Ag/AgCl. The diffractometry of the coating has revealed a preferential orientation toward the (220) plane. Nevertheless, the texture coefficient related to the (220) plane decreases as the potential increases due to the hydrogen evolution reaction. Also, the existence of uniform stress in the nickel coating electrodeposited from –0.60 V to –0.75 V was demonstrated according to peak displacement. For higher electrodeposition potentials, mechanical stress shifts to tensile stress.

ORCID

https://orcid.org/0000-0002-7562-3400 (Koutouan Desire Martial Abro)

Conflicts of Interest

The authors declare no conflicts of interest.

References

[1] R. Djouani and X. Qian. Mechanism of electrodeposition of nickel in aqueous solution. *Int. J. Curr. Res.* 2022, 10(01), 64228–64239.

[2] K. R. Mamaghani and S. M. Naghib. The effect of stirring rate on electrodeposition of nanocrystalline nickel coatings and their corrosion behaviors and mechanical characteristics. *Int. J. Electrochem. Sci.* 2017, 12(6), 023–5035. doi: 10.20964/2017.06.68.

[3] E. Gómez, R. Pollina, and E. Vallés. Nickel electrodeposition on different metallic substrates. *J. Electroanal. Chem.* 1995, 386, (1–2), 45.

[4] C. E. Dávalos, J. R. López, H. Ruiz, A. Méndez, R. A. López, and G. Trejo. Study of the Role of Boric Acid During the Electrochemical Deposition of Ni in a Sulfamate Bath. *Int. J. Electrochem. Sci.* 2013, 8, 9785–9800.

[5] A. Bund and D. Thiemig. Influence of bath composition and pH on the electrocodeposition of alumina nanoparticles and nickel. *Surf. Coatings Technol.* 2007, 201(16–17), 7092–7099. doi: 10.1016/j.surfcoat.2007.01.010.

[6] W. A. Thompson and H. J. Saxton. Structure, strength, and fracture of electrodeposited nickel and Ni−Co alloys. *Metall. Trans.*1973, 4(6) 1599–1605.

[7] M. Moharana and A. Mallik. Nickel electrocrystallization in different electrolytes: An in-process and post synthesis analysis. *Electrochim. Acta*. 2013, 98, 1–10.

[8] O. P. Watts. Rapid Nickel Plating. *Trans. Am. Electrochem. Soc.*1916, 29, 395.

[9] M. Monev, M. E. Baumgaertner, O. Leobich, and C. J. Raub. Innere Spannungen von kathodisch polarisierten Nickelschichten in schwefelsaueren Loesungen. *Metalloberflaeche*. 1991, 45, 77–85.

[10] E. L. Smith, A. P. Abbott, and K. S. Ryder. Deep Eutectic Solvents (DESs) and Their Applications. *Chem. Rev.* 2014, 114 (21), 11060–11082. doi: 10.1021/cr300162p.

[11] E. A. Mernissi Cherigui *et al*. Comprehensive Study of the Electrodeposition of Nickel Nanostructures from Deep Eutectic Solvents: Self-Limiting Growth by Electrolysis of Residual Water. *J. Phys. Chem. C*. 2017, 121(17), 9337–9347. doi: 10.1021/acs.jpcc.7b01104.

[12] L. P. Bonfrisco and M. Frary. Effects of crystallographic orientation on the early stages of oxidation in nickel and chromium. *J. Mater. Sci.* 2010, 45(6), 1663–1671. doi: 10.1007/s10853-009-4144-x.

[13] Y. Wang, L. Shen, M. Qiu, Z. Tian, X. Liu, and W. Zhuo. Jet Electrodeposition of Ni-SiO_2 Nanocomposite Coatings with Online Friction and Its Performance. *J. Electrochem. Soc.* 2016, 163(10) D579–D584. doi: 10.1149/2.0241610jes.

[14] L. N. Mendome. Surfaces nanostructurées de nickel électrodéposées sur divers substrats de dépôt: Etude de la croissance d'interface et des caractéristiques magnétiques. Université Reims Champagne, 2007.

[15] B. Scharifker and G. Hills. Theoretical and experimental studies of multiple nucleation. *Electrochim. Acta*. 1983, 28(7), 879–889.

[16] D. Grujicic and B. Pesic. Electrochemical and AFM study of nickel nucleation mechanisms on vitreous carbon from ammonium sulfate solutions. *Electrochim. Acta*. 2006, 51(13), 2678–2690. doi: 10.1016/j.electacta.2005.08.017.

[17] A. Ispas, H. Matsushima, A. Bund, and B. Bozzini. Nucleation and growth of thin nickel layers under the influence of a magnetic field. *J. Electroanal. Chem.* 2009, 626(1–2), 174–182. doi: 10.1016/j.jelechem.2008.12.015.

[18] A. N. Correia, S. A. Machado, and L. A. Avaca. Direct observation of overlapping of growth centres in Ni and Co electrocrystallisation using atomic force microscopy. *J. Electroanal. Chem.* 2000, 488(2), 110–116.

[19] M.-J. Deng, I.-W. Sun, P.-Y. Chen, J.-K. Chang, and W.-T. Tsai. Electrodeposition behavior of nickel in the water- and air-stable 1-ethyl-3-methylimidazolium-dicyanamide room-temperature ionic liquid. *Electrochim. Acta*. 2008, 53(19) 5812–5818. doi: 10.1016/j.electacta.2008.03.040.

[20] A. Milchev, Electrocrystallization, Fondamentals of Nucleation and Growth. Kluwer Acadamic Publishers, 2002.

[21] P. Scherrer, "Bestimmung der Grösse und der inneren Struktur von Kolloidteilchen mittels Röntgenstrahlen. *Nachr. Ges. Wiss. Göttingen*. 1918, 26. 98–100.

[22] R. T. C. Choo, J. M. Toguri, A. M. El-Sherik, and U. Erb. Mass transfer and electrocrystallization analyses of nanocrystalline nickel production by pulse plating. *J. Appl. Electrochem.* 1995, 25, 384–403.

[23] E. Rudnik, L. Burzyńska, and M. Gut. The effect of Cs^+ ions on codeposition of SiC particles with nickel. *Mater. Chem. Phys.* 2011, 26(3), 575. doi: 10.1016/j.matchemphys.2011.01.025.

[24] A. Azizi, A. Sahari, G. Schmerber, and A. Dinia. Nucleation and structural properties of nickel films electrodeposited from chloride and sulfate baths. *Int. J. Nanosci.*2008, 7(6) 345–352.

[25] E. Gòmez, R. Pollina, and E. Vallès. Nickel electrodeposition on different metallic substrates. *J. Electroanal. Chem.*1995, 386, 45–56.

[26] E. Gómez, R. Pollina, and E. Vallés. Morphology and structure of nickel nuclei as a function of the conditions of electrodeposition. *J. Electroanal. Chem.* 1995, 397(1–2) 111.

[27] C. Zanella, M. Lekka, and P. L. Bonora. Influence of the particle size on the mechanical and electrochemical behaviour of micro- and nano-nickel matrix composite coatings. *J. Appl. Electrochem.* 2008, 39(1), 31–38. doi: 10.1007/s10800-008-9635-y.

[28] K. Ngamchuea, S. Eloul, K. Tschulik, and R. G. Compton. Planar diffusion to macro disc electrodes — what electrode size is required for the Cottrell and Randles-Sevcik equations to apply quantitatively? 2014, 18, 3251–3257. doi: 10.1007/s10008-014-2664-z.

[29] A. Bewick, M. Fleischmann, and H. R. Thirsk. Kinetics of the electrocrystallization of thin films of calomel. *Trans. Faraday Soc.*1962, 58, 2200. doi: 10.1039/tf9625802200.

[30] Y. Wang, C. Weng, H. Sun, and B. Jiang. Tribological properties and corrosion resistance of nickel-based composite mold inserts containing lubricant nanoparticles for micro-injection molding. *J. Mater. Res. Technol.* 2023, 26, 5280–5293. doi: 10.1016/j.jmrt.2023.08.241.

[31] J. Amblard, M. Froment, and G. Maurin. Etude radiocristallographique de l'orientation préférentielle des dépôts électrolytiques de nickel. *Electrodepos. Surf. Treat.*1974, 2, 205–222.

[32] N. S. Qu, D. Zhu, K. C. Chan, and W. N. Lei. Pulse electrodeposition of nanocrystalline nickel using ultra narrow pulse width and high peak current density. *Surf. Coatings Technol.* 2003, 168(2–3), 123–128.

[33] C. B. Nielsen, A. Horsewell, and M. J. L. Østergàrd. On texture formation of nickel electrodeposits. *J. Appl. Electrochem.* 1997, 27(7), 839–845.

[34] A. Pandey, S. Dalal, S. Dutta, and A. Dixit. Structural characterization of polycrystalline thin films by X-ray diffraction techniques. *J Mater Sci Mater Electron*. 2021, 32, 1341–1368, 2021. doi: https://doi.org/10.1007/s10854-020-04998-w.

[35] A. A. Chernov. Theoretical and Technological Aspects of Crystal Growth," in *In: Materials Science Forum*, Rimini, Italy, 1998, 71–78.

[36] L. Vitos, A. V Ruban, H. L. Skriver, and J. Kolla. The surface energy of metals. *Surf.* Sci. 1998, 411, 186–202.

[37] L. Nzoghe-Mendome, A. Aloufy, J. Ebothé, D. Hui, and M. El Messiry. Surface roughening and transport properties in the growth of nano-structured nickel electrodeposits on ITO substrate. *Mater. Chem. Phys.* 2009, 115(2–3), 551–556. doi: 10.1016/j.matchemphys.2008.12.014.

[38] J. Amblard, M. Froment, and N. Spyrellis. Origine des textures dans les depots electrolytiques de nickel. *Surf. Technol.* 1977, 5 (3), 205–234.

[39] E. A. Pavlatou, M. Stroumbouli, P. Gyftou, and N. Spyrellis. Hardening effect induced by incorporation of SiC particles in nickel electrodeposits. *J. Appl. Electrochem.* 2006, 36(4), 385–394.

[40] T. Namazu and S. Inoue. Characterization of single crystal silicon and electroplated nickel films by uniaxial tensile test with in situ X-ray diffraction measurement. *Fatigue Fract. Eng. Mater. Struct.* 2007, 30(1), 13–20. doi: 10.1111/j.1460-2695.2006.01043.x.

[41] A. Khorsand Zak, W. H. Abd. Majid, M. E. Abrishami, and R. Yousefi. X-ray analysis of ZnO nanoparticles by Williamson-Hall and size-strain plot methods. *Solid State Sci.* 2011, 13, 251–256. doi: 10.1016/j.solidstatesciences.2010.11.024.